Non-perturbative calculation of molecular magnetic properties within current-density functional theory

E. I. Tellgren, A. M. Teale, J. W. Furness, K. K. Lange, U. Ekström, and T. Helgaker

Citation: The Journal of Chemical Physics **140**, 034101 (2014); doi: 10.1063/1.4861427
View online: http://dx.doi.org/10.1063/1.4861427
View Table of Contents: http://scitation.aip.org/content/aip/journal/jcp/140/3?ver=pdfcov
Published by the AIP Publishing

Non-perturbative calculation of molecular magnetic properties within current-density functional theory

E. I. Tellgren,[1,a)] A. M. Teale,[1,2,b)] J. W. Furness,[2] K. K. Lange,[1] U. Ekström,[1] and T. Helgaker[1]

[1]*Centre for Theoretical and Computational Chemistry, Department of Chemistry, University of Oslo, P.O. Box 1033 Blindern, N-0315 Oslo, Norway*

[2]*School of Chemistry, University of Nottingham, University Park, Nottingham NG7 2RD, United Kingdom*

(Received 9 October 2013; accepted 20 December 2013; published online 15 January 2014)

We present a novel implementation of Kohn–Sham density-functional theory utilizing London atomic orbitals as basis functions. External magnetic fields are treated non-perturbatively, which enable the study of both magnetic response properties and the effects of strong fields, using either standard density functionals or current-density functionals—the implementation is the first fully self-consistent implementation of the latter for molecules. Pilot applications are presented for the finite-field calculation of molecular magnetizabilities, hypermagnetizabilities, and nuclear magnetic resonance shielding constants, focusing on the impact of current-density functionals on the accuracy of the results. Existing current-density functionals based on the gauge-invariant vorticity are tested and found to be sensitive to numerical details of their implementation. Furthermore, when appropriately regularized, the resulting magnetic properties show no improvement over standard density-functional results. An advantage of the present implementation is the ability to apply density-functional theory to molecules in very strong magnetic fields, where the perturbative approach breaks down. Comparison with high accuracy full-configuration-interaction results show that the inadequacies of current-density approximations are exacerbated with increasing magnetic field strength. Standard density-functionals remain well behaved but fail to deliver high accuracy. The need for improved current-dependent density-functionals, and how they may be tested using the presented implementation, is discussed in light of our findings. [http://dx.doi.org/10.1063/1.4861427]

I. INTRODUCTION

Accurate and efficient calculation of magnetic properties is an important challenge for quantum-chemical methods. The effects of the magnetic fields available in laboratory experiments tend to be very weak compared with the natural energy scale for a small molecule, and so the dominant approach to the calculation of molecular magnetic properties has relied on the use of perturbation theory.[1,2] Both static and dynamic properties may be computed within this framework, although equations and implementations for high-order properties rapidly become unwieldy.

Recent work has developed an alternative, non-perturbative, gauge-origin-invariant approach to study molecules in magnetic fields,[3,4] without recourse to perturbation theory. Apart from offering a simple and convenient way to estimate static response quantities, this approach enables the study of molecules subject to very strong magnetic fields, for which a perturbation expansion converges very slowly, if at all.[4–6] In both perturbative and non-perturbative approaches, London atomic orbitals provide an efficient means of accelerating basis-set convergence by building part of the magnetic response and some gauge degrees of freedom into the basis functions. In particular, the use of London orbitals makes the calculations invariant to the choice of gauge origin for uniform magnetic fields.

While previous work was concerned with the Hartree–Fock[3] and full-configuration-interaction (FCI)[6] levels of theory, the present work explores the use of Kohn–Sham density-functional theory (KS-DFT) in magnetic fields. The standard formulation of KS-DFT is not rigorously valid in the presence of an external magnetic field. Instead, the theory needs to be generalized and some additional ingredient besides the charge density needs to be included in the universal exchange-correlation functional—either the magnetic field[7] or the current density.[8] We focus here on Vignale and Rasolt's formulation of current-density functional theory (CDFT), in which this extra ingredient is the paramagnetic current density.[8–10]

In practice, nearly all applications of DFT to molecular magnetic properties are performed with standard, density-dependent exchange-correlation functionals, often developed primarily for energetics in the absence of magnetic fields. As recently documented by comparison with high-accuracy coupled-cluster results for magnetizabilities and rotational g tensors[11] and for nuclear shielding and spin-rotation constants,[12] the accuracy achieved by such Kohn–Sham calculations is rather low. For many exchange-correlation functionals, the Kohn–Sham results are no better than the Hartree–Fock results and never better than the CCSD results. It has been suggested that the use of CDFT may lead to improved results.

a)Electronic mail: erik.tellgren@kjemi.uio.no
b)Electronic mail: andrew.teale@nottingham.ac.uk

In this paper, we present an implementation of (C)DFT using London atomic orbitals. We commence in Sec. II by presenting the theoretical modifications to KS-DFT necessary in the presence of a magnetic field, focusing on the Vignale–Rasolt (VR) formulation of CDFT and the associated vorticity-dependent exchange-correlation functionals available in the literature. In Sec. III, we present our implementation of a (C)DFT module in the LONDON program, capable of performing both standard DFT and CDFT calculations in the presence of magnetic fields. Results using CDFT are presented in Sec. IV for magnetic properties typically accessible by response theory. Comparisons of these results with recent benchmark data and those from standard DFT calculations allow us to assess the quality of the different CDFT functionals. In Sec. V, we extend our study to field strengths where response theory is no longer applicable; in this regime, the results are compared with those obtained from FCI calculations. Finally, in Sec. VI, we make some concluding remarks and discuss directions for future work.

II. THEORY

In the present section, we first consider the Vignale–Rasolt formulation of CDFT in Sec. II A; next, we consider the Vignale, Rasolt, and Geldart (VRG) functional and its parameterizations in Sec. II B.

A. The Vignale–Rasolt universal CDFT functional

In the presence of a magnetic field, the non-relativistic electronic Hamiltonian takes the form (atomic units)

$$\hat{H}[v,\mathbf{A}] = \frac{1}{2}\sum_{k=1}^{N}(\hat{\mathbf{p}}_k + \mathbf{A}(\mathbf{r}_k))^2 + \sum_{k=1}^{N} v(\mathbf{r}_k) + \frac{1}{2}\sum_{k\neq l}^{N}\frac{1}{r_{kl}}, \tag{1}$$

where N is the number of electrons, $\hat{\mathbf{p}}_k$ is the canonical-momentum operator of electron k, $v(\mathbf{r})$ is the external scalar potential at position $\mathbf{r}$, and the magnetic vector potential $\mathbf{A}(\mathbf{r})$ describes the external magnetic field $\mathbf{B}(\mathbf{r}) = \nabla \times \mathbf{A}(\mathbf{r})$. In CDFT, the electronic ground-state energy may then be expressed as follows,[8]

$$\begin{aligned} E[v,\mathbf{A}] &= \inf_{\psi}\langle\psi|\hat{H}[v,\mathbf{A}]|\psi\rangle \\ &= \inf_{\rho,\mathbf{j}_\mathrm{p}}\left(F[\rho,\mathbf{j}_\mathrm{p}] + \int\left(\rho v + \tfrac{1}{2}\rho A^2 + \mathbf{j}_\mathrm{p}\cdot\mathbf{A}\right)\mathrm{d}\mathbf{r}\right), \end{aligned} \tag{2}$$

where ρ is the electron density, $\mathbf{j}_\mathrm{p}$ is the paramagnetic current density, and $F[\rho,\mathbf{j}_\mathrm{p}]$ is the Vignale–Rasolt constrained-search universal current-density functional:

$$F[\rho,\mathbf{j}_\mathrm{p}] = \inf_{\psi\mapsto\rho,\mathbf{j}_\mathrm{p}}\langle\psi|\hat{H}[0,0]|\psi\rangle. \tag{3}$$

In Kohn–Sham theory, this functional may be decomposed further into a Kohn–Sham noninteracting kinetic-energy term $T_\mathrm{s}[\rho,\mathbf{j}_\mathrm{p}]$, a Hartree term $J[\rho]$, and an exchange-correlation term $F_\mathrm{xc}[\rho,\mathbf{j}_\mathrm{p}]$:

$$F[\rho,\mathbf{j}_\mathrm{p}] = T_\mathrm{s}[\rho,\mathbf{j}_\mathrm{p}] + J[\rho] + F_\mathrm{xc}[\rho,\mathbf{j}_\mathrm{p}]. \tag{4}$$

From gauge-invariance considerations, Vignale and Rasolt[8,9] argued that the exchange-correlation energy depends only on $\mathbf{j}_\mathrm{p}$ through the gauge-invariant vorticity,

$$\begin{aligned} \boldsymbol{\nu}(\mathbf{r}) &= \nabla\times\frac{\mathbf{j}_\mathrm{p}(\mathbf{r})}{\rho(\mathbf{r})} \\ &= \frac{\rho(\mathbf{r})\nabla\times\mathbf{j}_\mathrm{p}(\mathbf{r}) - \nabla\rho(\mathbf{r})\times\mathbf{j}_\mathrm{p}(\mathbf{r})}{\rho(\mathbf{r})^2}. \end{aligned} \tag{5}$$

In the expressions given above, the spin degrees of freedom and the spin-Zeeman term have been neglected. The literature contains slightly different formalisms for taking these into account. In particular, F and F_xc have been considered functionals of the following variables:

(1) the total density ρ, the spin density $\mathbf{m}$, and the total paramagnetic current density $\mathbf{j}_\mathrm{p}$,
(2) the total density ρ and the total paramagnetic current-spin density $\mathbf{j}_\mathrm{m} = \mathbf{j}_\mathrm{p} + \nabla\times\mathbf{m}$,[13]
(3) the fully spin-resolved densities $\rho_\uparrow$ and $\rho_\downarrow$ and paramagnetic current densities $\mathbf{j}_{\mathrm{p};\uparrow}$ and $\mathbf{j}_{\mathrm{p};\downarrow}$.[9]

The choice between spin-resolved or total densities matters in particular for the vorticity, which is not additive with respect to spins, $\boldsymbol{\nu}_\mathrm{tot} \neq \boldsymbol{\nu}_\uparrow + \boldsymbol{\nu}_\downarrow$ and which vanishes identically for densities arising from a single natural orbital (or Kohn–Sham orbital). Hence, it is possible for $\boldsymbol{\nu}_\mathrm{tot} \neq 0$, yet $\boldsymbol{\nu}_\uparrow \equiv \boldsymbol{\nu}_\downarrow \equiv 0$ (e.g., for a two-electron system in a triplet spin state). In the present work, we apply existing approximate functionals to closed-shell systems, for which these distinctions do not matter. We, therefore, suppress spin indices in the following.

The fact that vorticities arising from a single orbital vanish identically raises the question as to which paramagnetic densities $(\rho,\mathbf{j}_\mathrm{p})$ can be represented by a Kohn–Sham ground-state wave function. Clearly, a closed-shell two-electron system with a nonzero total vorticity is neither non-interacting v-representable nor N-representable by a Kohn–Sham system. Moreover, an open-shell two-electron system may feature non-vanishing spin vorticities, which also cannot be represented by a Kohn–Sham system; see also Taut *et al.* for a discussion of non-interacting v-representability in two-electron systems.[14] For $N \geq 4$ electrons, a recent result shows that all paramagnetic densities satisfying mild regularity conditions are non-interacting N-representable.[15] Depending on how the question of non-interacting N-representability is resolved for few-particle systems and how non-interacting v-representability is resolved for $N \geq 3$, a rigorous approach to CDFT may require extended (ensemble) Kohn–Sham theory and the use of methods for determining fractional occupation numbers.[16–19] It has recently been proved that essentially any density and paramagnetic current density (subject only to the minimal regularity condition that a von Weizsäcker-like bound on the kinetic energy is locally integrable) are N-representable in extended Kohn–Sham CDFT.[20]

B. The VRG exchange-correlation functional

Compared with the very large number of DFT exchange-correlation functionals, there exist only a handful of specific

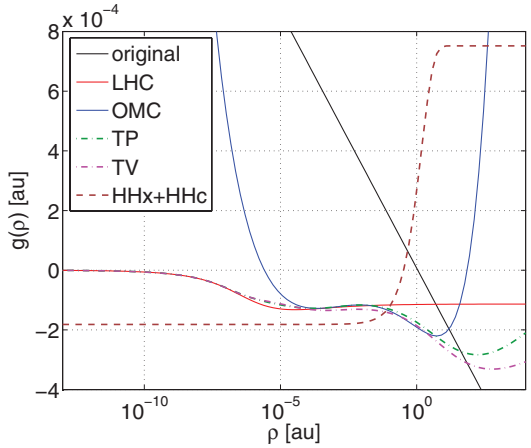

FIG. 1. Different model functions $g(\rho)$ used in the VRG functional.

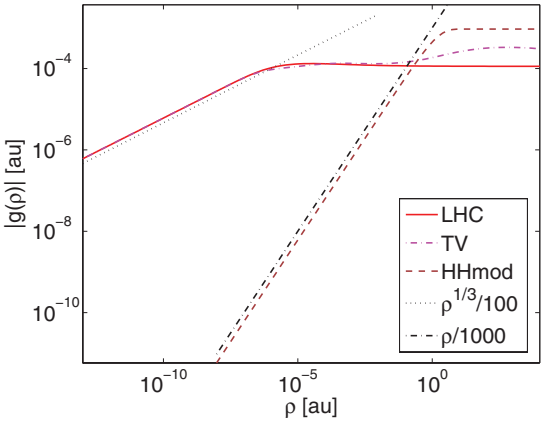

FIG. 2. The low-density behaviour of three model functions $g(\rho)$ used in the VRG functional. The Higuchi–Higuchi exchange functional HHx has been reparametrized so that the total exchange-correlation functional approaches zero for small densities; however, the correlation functional HHc goes through a singularity and a sign shift at $\rho = 10^{-30}$ a.u. The indicated asymptotic HHx+HHc behaviour therefore does not extend to this region.

CDFT functionals. Some of these are based on the vorticity expansion and take the general form

$$F_{\mathrm{VRG}}[\rho, \boldsymbol{v}] = \int g(\rho(\mathbf{r}))\, |\boldsymbol{v}(\mathbf{r})|^2 \, \mathrm{d}\mathbf{r}, \tag{6}$$

where approximations to $g(\rho)$ have been established from models of the uniform electron gas. Indeed, such a functional form was considered by Vignale and Rasolt already in Ref. 8 and subsequently fitted to reference values computed with the random-phase approximation (RPA) by Vignale, Rasolt, and Geldart in Ref. 21.

This original parameterization has been revisited several times—specifically, re-parameterizations have been proposed by Lee, Handy, and Colwell (LHC),[22,23] by Orestes, Marcasso, and Capelle (OMC),[24] by Tao and Perdew (TP),[25] and by Tao and Vignale (TV).[26] Additionally, Higuchi and Higuchi (HH)[27,28] have constructed an approximate exchange-correlation functional designed to satisfy exact conditions derived from scaling relations for the CDFT exchange and correlation energies.

For molecules, it is essential that the parameterization of the VRG functional has a sensible low-density limit. However, in the above parameterizations, fitting reference data for $g(\rho)$ were available only for Wigner–Seitz radii in the range $0 < r_s \leq 10$ (VRG, LHC, OMC, TP) and in the range $0 < r_s \leq 20$ (TV). The low-density limit is consequently underdetermined by the reference data.

The low-density behaviour of the different parametrizations is shown in Fig. 1. Importantly, the original VRG form and the OMC re-parametrization do not tend to zero in the low-density limit, making them ill-suited for molecular applications. By contrast, the LHC, TP, and TV re-parametrizations do tend to zero, albeit slowly—for sufficiently small ρ, we find that

$$g_{\mathrm{LHC}}(\rho) \approx g_{\mathrm{TP}}(\rho) \approx g_{\mathrm{TV}}(\rho) \sim -\rho^{1/3}. \tag{7}$$

For the LHC and TV re-parameterizations, which result in everywhere negative functions $g_{\mathrm{LHC}}(\rho)$ and $g_{\mathrm{TV}}(\rho)$, respectively, this decay behaviour is readily visualized in a log–log plot; see Fig. 2 (the TP parametrization is not shown as it differs very little from the TV parameterization on the scale of the plot and the low-density asymptotes coincide).

Higuchi and Higuchi's exchange functional HHx is constant: $g_{\mathrm{HHx}}(\rho) = 2 \times 3.76 \times 10^{-4}$ a.u. By adjusting this constant (i.e., setting $\bar{D}_x = -\bar{C}_0$ in the notation of Ref. 27), it is possible to make their total $g_{\mathrm{HH}}(\rho)$ almost vanish for small densities $\rho \gg 10^{-30}$ a.u; see Fig. 2. However, the Higuchi–Higuchi correlation functional HHc has a singularity at $\rho = 10^{-30}$ a.u., so the approach to the low-density limit is interrupted by an infinite. We denote the modified Higuchi–Higuchi functional by HHmod.

Finally, we note that Zhu and Trickey[29] compared vorticity-dependent functionals with an exactly solvable model for a Hooke's atom in a magnetic field, reporting that the vorticity is a difficult quantity to work with. An alternative approach has been proposed by Becke,[30] while a more elaborate version (relying on currents from individual Kohn–Sham orbitals) was proposed by Pittalis *et al.*[31] These functionals are based on the observation that a gauge-invariant density can be formed from a combination of the Kohn–Sham canonical-kinetic-energy density and the paramagnetic current density. Letting ϕ_k denote the occupied Kohn–Sham orbitals that give rise to the densities ρ and $\mathbf{j}_{\mathrm{p}}$, the quantity

$$\widetilde{\tau}(\mathbf{r}) = \tfrac{1}{2} \sum_k |\nabla \phi_k(\mathbf{r})|^2 - \frac{|\mathbf{j}_{\mathrm{p}}(\mathbf{r})|^2}{2\rho(\mathbf{r})} \tag{8}$$

is gauge invariant.[32] The paramagnetic current can therefore be incorporated in an exchange-correlation functional via $\widetilde{\tau}$. Exploration of this alternative is beyond the scope of the present work.

III. IMPLEMENTATION

In our calculations, we consider a uniform magnetic field $\mathbf{B}$, described by a cylindrical vector potential

$$\mathbf{A}(\mathbf{r}) = \frac{1}{2}\mathbf{B} \times (\mathbf{r} - \mathbf{g}), \tag{9}$$

where **g** is the gauge origin. In exact calculations, with complete orbital basis sets, the values of physical quantities are independent of the gauge origin (in fact, invariant to all gauge transformations). For finite basis sets, gauge-origin invariance can be ensured by employing London orbitals of the form

$$\omega_\gamma(\mathbf{r}) = \chi_\gamma(\mathbf{r})\, \mathrm{e}^{-\mathrm{i}\mathbf{A}(\mathbf{N}_\gamma)\cdot\mathbf{r}}, \tag{10}$$

where $\chi_\gamma(\mathbf{r})$ is a standard Gaussian-type basis function centred on $\mathbf{N}_\gamma$ and $\mathbf{A}(\mathbf{N}_\gamma)$ is the vector potential evaluated at the centre of the Gaussian. Effectively, the basis then becomes a hybrid plane-wave/Gaussian basis for finite magnetic fields.[3]

The main modifications to the existing LONDON Hartree–Fock code[3] in order to enable (C)DFT calculations are the implementation of a numerical integration scheme, the evaluation of quantities such as $\rho(\mathbf{r})$, $\nabla\rho(\mathbf{r})$, $\mathbf{j}_\mathrm{p}(\mathbf{r})$, and $\boldsymbol{\nu}(\mathbf{r})$ on the associated numerical grid and the assembly of these components in the expressions for the exchange-correlation energies and the functional derivatives required for their associated potentials.

For the molecular numerical integration, we construct a set of grid points and weights using Becke's space partitioning scheme with atomic size corrections,[33] decomposing the molecular integral into a sum of one-centre atom-like integrals. To eliminate crowding of points close to nuclei, grid pruning is implemented using the approach outlined by Murray, Handy, and Laming.[34] For the radial part of these integrations, we employ the scheme proposed by Lindh, Malmqvist, and Gagliardi (LMG);[35] for the angular part, we employ Lebedev quadrature.[36–41] We have tested our C++ implementation for standard density functionals by comparing with the DALTON quantum chemistry program,[42,43] in which similar Fortran 77 angular and radial implementations are available. Because of the slow decay of the vorticity-dependent integrand in the present VRG parameterizations, we have used very conservative screening criteria when processing points on the integration grid.

The evaluation of $\rho(\mathbf{r})$, $\nabla\rho(\mathbf{r})$, $\mathbf{j}_\mathrm{p}(\mathbf{r})$, and $\boldsymbol{\nu}(\mathbf{r})$ at the grid points is straightforward, given the elements of the one-particle reduced density matrix $D^{\gamma\zeta}$ and the values of basis functions $\omega_\gamma(\mathbf{r})$ and their gradients $\nabla\omega_\gamma(\mathbf{r})$ at the grid points:

$$\rho(\mathbf{r}) = \sum_{\gamma\zeta} \omega_\gamma(\mathbf{r})\, D^{\gamma\zeta}\, \omega^*_\zeta(\mathbf{r}), \tag{11}$$

$$\nabla\rho(\mathbf{r}) = \sum_{\gamma\zeta} \omega_\gamma(\mathbf{r})\, D^{\gamma\zeta}\, \nabla\omega^*_\zeta(\mathbf{r}) + \mathrm{c.c.}, \tag{12}$$

$$\mathbf{j}_\mathrm{p}(\mathbf{r}) = \frac{\mathrm{i}}{2} \sum_{\gamma\zeta} \omega_\gamma(\mathbf{r})\, D^{\gamma\zeta}\, \nabla\omega^*_\zeta(\mathbf{r}) + \mathrm{c.c.}, \tag{13}$$

where "c.c." denotes the complex conjugate of the preceding expression. (Note that we work with the *number* density and *number* current rather than the *electrical* density and *electrical* current, the difference being a factor of $-\mathrm{e}$ in general, or -1 in atomic units.) Notably, the curl of $\mathbf{j}_\mathrm{p}$ can be computed from the first-order functional derivatives of basis functions since the second-order derivatives cancel:

$$\nabla \times \mathbf{j}_\mathrm{p}(\mathbf{r}) = \mathrm{i} \sum_{\gamma\zeta} D^{\gamma\zeta}\, \nabla\omega_\gamma(\mathbf{r}) \times \nabla\omega^*_\zeta(\mathbf{r}). \tag{14}$$

At first glance, the right-hand side looks like an imaginary quantity; however, for a complex vector **w**, the cross-product $\mathrm{i}\mathbf{w} \times \mathbf{w}^*$ is real. A transformation to natural orbitals (or Kohn–Sham orbitals) thus makes it clear that the right-hand side is real.

The vorticity may be assembled from the above densities using the right-hand side of Eq. (5) above. In practice, to guard against division by near-zero, we prefer the regularized vorticity

$$\boldsymbol{\nu}_\epsilon(\mathbf{r}) = \frac{\rho(\mathbf{r})\nabla \times \mathbf{j}_\mathrm{p}(\mathbf{r}) - \nabla\rho(\mathbf{r}) \times \mathbf{j}_\mathrm{p}(\mathbf{r})}{\sqrt{\epsilon^4 + \rho(\mathbf{r})^4}}, \tag{15}$$

where ϵ plays the role of a soft density cut-off. This regularization results in an underestimate of the magnitude of the true vorticity.

Once the required (C)DFT quantities have been assembled at the grid points, the exchange-correlation energies and the derivatives required for construction of their associated Kohn–Sham matrix contributions can be calculated. For the standard DFT contributions, we use the flexible XCFUN package,[44] which uses automatic differentiation to provide derivatives of the exchange-correlation energies from specified energy expressions. Once these contributions have been evaluated, LONDON constructs the associated Kohn–Sham matrix elements.

For the CDFT contributions (which in the present work are added as corrections to standard functionals), we have implemented the exchange-correlation energy and Kohn–Sham matrix element constructions in the LONDON code. For $F_{\mathrm{VRG(LHC)}}$ and $F_{\mathrm{VRG(TV)}}$, which have everywhere negative integrands, the regularization of Eq. (15) is used and the corresponding vorticity correction is therefore underestimated—at least when applied non-self-consistently. For VRG parameterizations that decay as $\rho^{1/3}$ in the low-density limit, the regularization in Eq. (15) yields a VRG integrand of the form

$$g(\rho)\nu_\epsilon^2 \sim -\rho^{1/3} \frac{\left|\rho\nabla \times \mathbf{j}_\mathrm{p} - \nabla\rho \times \mathbf{j}_\mathrm{p}\right|^2}{\epsilon^4 + \rho^4}. \tag{16}$$

Without regularization (i.e., with $\epsilon = 0$), this decay may be numerically problematic—in regions where the vorticity vanishes or is very small, numerical noise in the squared factor would be amplified by a factor $\rho^{-11/3}$. The need for appropriate regularization of the vorticity has been noted in Ref. 45. The sensitivity of calculated properties to the choice of the regularization parameters is investigated in Sec. IV.

IV. (C)DFT IN THE PERTURBATIVE REGIME

Over the last two decades, perturbative calculations of second-order properties such as magnetizabilities and nuclear shielding constants have become routine in quantum chemistry, also with London atomic orbitals. Properties that require higher-order responses such as hypermagnetizabilities have received much less attention. Perturbative approaches have been applied at the coupled-perturbed Hartree–Fock level using standard (non-London) orbitals by Pagola *et al.*,[46,47] while the finite-difference approach has been explored by us at the Hartree–Fock level using London orbitals.[3] However, we

are not aware of any results for hypermagnetizabilities that employ methods including a correlation treatment.

In this section, we present applications of CDFT to magnetizabilities, fourth-rank hypermagnetizabilities, and nuclear shielding constants. The implementation of molecular properties is much simpler by finite-field techniques than that by perturbation techniques, allowing us to assess readily the performance of a variety of CDFT functionals, comparing their results with Hartree–Fock theory, the corresponding DFT functionals and (where available) accurate benchmark data.

We have performed calculations on a set of 27 molecules used in Ref. 12 at their CCSD(T)/cc-pVTZ optimized geometries, namely, AlF, C_3H_4 (cyclopropene), FCCH, C_2H_4, H_2C_2O (ketene), CH_3F, CH_4, CO, FCN, HCN, HCP, HF, LiH, LiF, NH_3, N_2, N_2O, PN, H_4C_2O (oxirane), OCFH, CH_2O (formaldehyde), OCS, OF_2, HOF, H_2O, H_2S, and SO_2 (O_3 has been excluded because of its multi-reference character). In all cases the aug-cc-pCVTZ London atomic orbital basis set has been employed. The CDFT vorticity dependent functionals were regularized with a hard cut-off on the Wigner–Seitz radius, r_s, of 9.1055 a.u. and a soft cut-off $\epsilon = 10^{-14}$ a.u., see Eq. (15). Experimentation revealed that results were not particularly sensitive to the angular or radial grid parameters. The default parameters were therefore used. For the Lebedev grid, the angular integration was specified to be exact for spherical harmonics up to order 35; in the LMG radial integration, the accuracy parameter specifying the upper limit of the error in the case of an atomic integration was set to 10^{-13} a.u.

Even when employing the regularization of Eq. (15) issues with self-consistent-field (SCF) convergence were still encountered for the VRG(LHC) parameterized CDFT corrections at some field strengths, when employing the standard direct-iteration-in-the-iterative-subspace (DIIS) approach. Interestingly, no such issues were encountered with the VRG(TP) parameterization, for which calculations on the full set of 27 molecules could be routinely performed at a range of field strengths up to 1 a.u. This may reflect differences in the function $g(\rho)$ examined in Figures 1 and 2. In particular, the 8 molecules CH_3F, HCN, HCP, H_4C_2O, CH_2O, OCS, OF_2, and SO_2 could not be reliably converged using the VRG(LHC) parameterization. To account for this all plots and error analyses in the main manuscript refer to the remaining subset of 19 molecules. The full data set may be found in the supplementary material,[48] including VRG(TP) based results for all 27 molecules. We emphasize that some regularization is necessary for all of the VRG based forms; even for VRG(TP) applying less regularization leads to similar numerical difficulties. We observe that these issues are, however, somewhat less severe with the VRG(TP) parameterization than with the VRG(LHC) parameterization.

A. Molecular magnetizabilities and hypermagnetizabilities

Consider a uniform magnetic field **B** whose vector potential is given by Eq. (9). Expanding the energy in orders of **B**, we obtain for a closed-shell system,

$$E(\mathbf{B}) = E(\mathbf{0}) - \frac{1}{2}\sum_{\alpha\beta}\chi_{\alpha\beta}B_\alpha B_\beta - \frac{1}{4!}\sum_{\alpha\beta\gamma\zeta}X_{\alpha\beta\gamma\zeta}B_\alpha B_\beta B_\gamma B_\zeta + \mathcal{O}(B^6), \quad (17)$$

where odd-order terms vanish. The magnetizability tensor $\chi_{\alpha\beta}$ and fourth-rank hypermagnetizability tensor $X_{\alpha\beta\gamma\zeta}$ can be obtained by least-squares fitting of a polynomial to energies $E(\mathbf{B}_{\alpha\ell})$ for a suitable discrete grid of sample fields $\mathbf{B}_{\alpha\ell}$. We consider here only the diagonal tensor elements (which require less fitting data), using $\mathbf{B}_{\alpha\ell} = \ell\mathbf{e}_\alpha$. It was found that $\ell = 0.00, 0.01, \ldots, 0.03$ a.u. in each Cartesian direction, $\alpha \in \{x, y, z\}$ provided sufficient data to accurately determine molecular magnetizabilities and shielding constants; the results reproducing those of the perturbative DALTON[42,43] implementation to better than 0.1×10^{-30} JT^{-2} and 0.1 ppm, respectively, for standard density functionals. Careful study of the convergence of hypermagnetizabilities revealed that higher field strengths were required to obtain robust results and the grids used were supplemented with the points $\ell = 0.03, 0.04, \ldots, 0.1$ a.u. in each Cartesian direction, making the calculations considerably more expensive. The tensor elements were calculated by fitting 6th-order polynomials in each Cartesian direction.

In a previous benchmark study of magnetizabilities and g tensors calculated from standard DFT functionals, Lutnæs *et al.* found that the standard DFT functionals (which neglect the current dependence) in general give poorer results than does the Hartree–Fock model.[11] Moreover, whereas the Hartree–Fock model (like the coupled-cluster models) on average underestimates magnetizabilities, the local density approximation (LDA) and generalized gradient approximation (GGA) functionals overestimate the magnetizabilities. In Fig. 3, we have plotted the magnetizabilities obtained

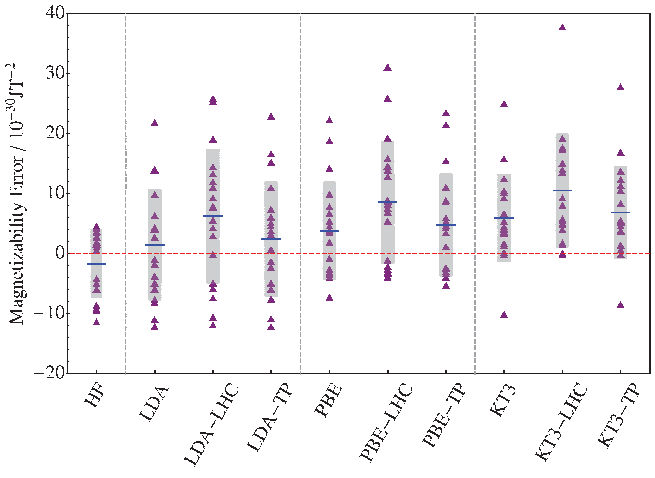

FIG. 3. Illustration of the errors in isotropic molecular magnetizabilities (10^{-30} JT^{-2}) calculated using DFT functionals with and without the VRG(LHC) and VRG(TP) corrections in the aug-cc-pCVTZ basis set. Results that failed to converge during SCF optimization with the VRG(LHC) corrections have been omitted. The grey boxes enclose one sample standard deviation above and below the mean error. The mean error for each method is indicated by a horizontal blue line. The plot markers show the individual errors for each of the 19 molecules listed in Sec. IV.

TABLE I. Hypermagnetizability tensor elements (SI a.u.) calculated using DFT functionals in the aug-cc-pCVTZ basis set. The corresponding Hartree–Fock results are included for comparison. Results are presented here for the subset of 19 molecules described in Sec. IV. Data for the full set of 27 molecules may be found in the supplementary material.[48]

	HF			KT3			PBE		
	xxxx	yyyy	zzzz	xxxx	yyyy	zzzz	xxxx	yyyy	zzzz
AlF	94.9	94.9	91.0	90.9	90.9	95.5	84.7	84.7	95.7
C_3H_4	− 3.8	− 250.0	222.0	45.0	− 300.0	233.0	25.3	− 297.0	223.0
FCCH	− 9.6	− 9.6	40.3	− 19.0	− 19.0	45.8	− 21.6	− 21.6	45.8
C_2H_4	− 60.1	− 41.1	− 4.6	− 50.4	− 70.9	− 45.0	− 69.9	− 91.7	− 43.5
H_2C_2O	− 1.3	− 94.4	228.0	− 6.8	− 115.0	252.0	− 10.6	− 113.0	259.0
CH_4	91.0	91.1	100.0	104.0	104.0	115.0	105.0	105.0	116.0
CO	− 6.4	− 6.4	17.5	15.8	15.8	21.2	9.9	9.9	21.8
FCN	− 10.1	− 10.1	23.4	− 12.6	− 12.6	26.6	− 16.0	− 16.0	26.7
HF	7.9	7.9	5.7	11.8	11.8	8.8	11.9	11.9	9.2
LiH	75.1	75.1	67.9	160.0	160.0	94.9	157.0	157.0	97.4
LiF	4.9	4.9	12.7	41.7	41.7	26.7	35.3	35.3	26.8
NH_3	38.9	38.9	50.7	49.2	49.2	60.3	49.3	49.3	61.0
N_2	− 16.7	− 16.7	15.8	6.4	6.4	17.8	− 1.7	− 1.7	18.2
N_2O	− 69.6	− 69.6	19.1	− 81.6	− 81.6	21.8	− 85.3	− 85.3	22.2
PN	− 230.0	− 230.0	56.2	− 294.0	− 294.0	57.0	− 381.0	− 381.0	57.4
HFCO	16.4	− 20.5	− 65.2	22.4	− 18.9	− 49.3	27.1	− 26.2	− 66.1
HOF	29.9	26.6	15.9	6.1	− 12.7	24.4	5.1	− 18.7	24.9
H_2O	22.3	14.8	13.5	30.6	21.5	21.7	30.7	21.8	21.8
H_2S	197.0	81.7	117.0	206.0	90.0	124.0	209.0	90.4	125.0

using the conventional LDA, Perdew, Burke, and Ernzerhof (PBE),[63] and Keal and Tozer (KT3)[64] functionals without current correction and with the VRG(LHC) and VRG(TP) corrections; for comparison, we have included the Hartree–Fock results for the same systems. We see the same trends as observed in Ref. 11, the LDA, PBE, and KT3 functionals overestimating the magnetizabilities and being less systematic than the Hartree–Fock model.

Unfortunately, the addition of the VRG functional (with the LHC and TP parameterizations) does not improve the situation. For all three DFT functionals, the VRG(LHC) correction increases the error in the magnetizabilities, increasing both mean errors and the spread. The results are slightly better for the VRG(TP) functional but still poorer than those obtained without the VRG correction. Clearly, the VRG-corrected functionals cannot be recommended for the calculation of magnetizabilities. We note that Lee, Collwell, and Handy[22] studied magnetizabilities for a few small systems in the context of CDFT using a perturbative implementation. Many of the systems they considered are included in the present work, however, a direct comparison is difficult because of the use of different basis sets and the fact that the results of Ref. 22 are not gauge-origin invariant. The present results may therefore be considered a more extensive benchmark addressing some of the issues associated with these earlier calculations.

In Table I, we have listed the hypermagnetizabilities calculated at the Hartree–Fock, KT3, and PBE levels of theory, all without VRG corrections; the corresponding VRG-corrected results may be found in the supplementary material.[48] To our knowledge, these are the first published Kohn–Sham hypermagnetizabilities.

We observe an overall qualitative agreement between the KT3 and PBE hypermagnetizabilities—except for N_2 and HFCO, the results agree on signs and relative magnitudes. As expected, the agreement with the uncorrelated Hartree–Fock model is poorer, with more instances of sign differences. However, without high-quality reference data (such as those provided by coupled-cluster theory), it is difficult to assess properly the performance of the Hartree–Fock and Kohn–Sham DFT models for hypermagnetizabilities.

We have carried out Kohn–Sham calculations of hypermagnetizabilities with the VRG correction added; the results are included in the supplementary material.[48] In nearly all cases, the VRG correction to the hypermagnetizability tensor elements is negative; however, in the absence of accurate reference data, it is difficult to judge the quality of the CDFT results for the hypermagnetizabilities. Bearing in mind the poor performance of the VRG correction for magnetizabilities, it is a safe assumption that the hypermagnetizability corrections are poor as well.

B. Nuclear shielding constants

In a recent benchmark study of nuclear magnetic resonance (NMR) shielding constants and spin-rotation constants,[12] the accuracy achieved by Kohn–Sham calculations was found to be rather low. Although the various DFT approximations improve slightly upon the Hartree–Fock results, none of the DFT functionals provide an accuracy similar to that of CCSD or CCSD(T) theory; moreover, the inclusion of vibrational corrections worsened the agreement with experimental values. Regarding the different exchange-correlation functionals, a general improvement was observed when going from LDA to GGA functionals, with further

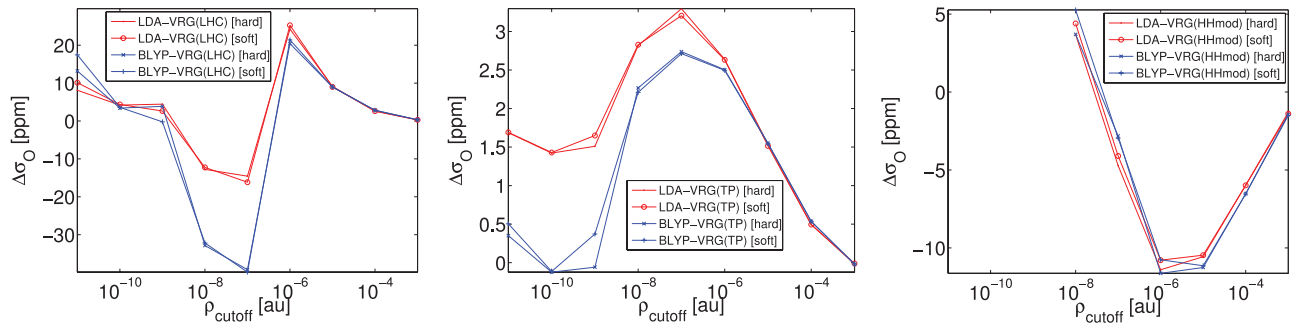

FIG. 4. The VRG correction to the oxygen shielding constant in the water molecule plotted against the integration regularization cut-off parameter $\rho_{\text{cut-off}}$ for the LHC (left), TP (middle), and HHmod (right) parameterizations of $g(\rho)$ in Eq. (6). Both hard and soft cut-offs are illustrated in the plots. The Huz-II basis, with London gauge factors, was used in all cases.

improvements observed for hybrid functionals—in particular, in combination with an optimized-effective-potential (OEP) approach. Interestingly, KS[CCSD] and KS[CCSD(T)] calculations, where the Kohn–Sham system reproduces the CCSD and CCSD(T) densities, respectively, gave errors similar to those of the OEP calculations. This suggested that the neglect of current dependence may be a significant factor in determining the accuracy of these calculations.

To calculate NMR shielding constants non-perturbatively we consider the dependence of the molecular electronic energy $E(\mathbf{B}, \mathbf{M}_k)$ on the external magnetic field $\mathbf{B}$ and the nuclear magnetic moment $\mathbf{M}_k$ of nucleus k represented by the vector potential,

$$\mathbf{A}_k(\mathbf{r}) = \frac{\mu_0}{4\pi}\frac{\mathbf{M}_k \times (\mathbf{r}-\mathbf{K})}{|\mathbf{r}-\mathbf{K}|^3} = \frac{\mu_0}{4\pi}\mathbf{M}_k \times \frac{1}{\partial \mathbf{K}}\frac{1}{|\mathbf{r}-\mathbf{K}|}, \quad (18)$$

where $\mathbf{K}$ is the position of the nucleus. We obtain the Taylor expansion

$$E(\mathbf{B}, \mathbf{M}_k) = E(\mathbf{0}, \mathbf{0}) + \sum_{\alpha\beta} \sigma_{k;\alpha\beta} B_\alpha M_{k;\beta} + \cdots, \quad (19)$$

where the nuclear shielding tensor is the leading-order mixed term in the expansion of the energy,

$$\sigma_{k;\alpha\beta} = \frac{\partial^2 E(\mathbf{B}, \mathbf{M}_k)}{\partial B_\alpha \partial M_{k;\beta}}\Big|_{\mathbf{B}=\mathbf{0},\mathbf{M}_k=\mathbf{0}}. \quad (20)$$

The kinetic-energy operator in the Hamiltonian now becomes (atomic units) $\hat{\pi}^2/2 = (\hat{\mathbf{p}} + \mathbf{A}(\mathbf{r}) + \mathbf{A}_k(\mathbf{r}))^2/2$. Exploiting the Hellmann–Feynman theorem, we compute the derivative with respect to $\mathbf{M}_k$ analytically,

$$\begin{aligned}\Xi_{k;\beta}(\mathbf{B}) &= \frac{\partial E(\mathbf{B}, \mathbf{M}_k)}{\partial M_{k;\beta}}\Big|_{\mathbf{M}_k=\mathbf{0}} \\ &= \frac{e\mu_0}{4\pi m}\epsilon_{\alpha\beta\gamma}\frac{\partial}{\partial K_\gamma}\langle\psi|\left\{\hat{p}_\alpha + eA_\alpha, |\mathbf{r}-\mathbf{K}|^{-1}\right\}|\psi\rangle,\end{aligned} \quad (21)$$

where the braces denote the anti-commutator. The expectation value is similar to a nuclear attraction integral, and may be evaluated using the McMurchie–Davidson scheme described in previous work.[3] The remaining differentiation may be performed directly by numerical differentiation,

$$\sigma_{k;\alpha\beta} \approx \frac{\Xi_{k;\beta}(\epsilon\mathbf{e}_\alpha) - \Xi_{k;\beta}(-\epsilon\mathbf{e}_\alpha)}{2\epsilon} = \frac{\Xi_{k;\beta}(\epsilon\mathbf{e}_\alpha)}{\epsilon}, \quad (22)$$

or indirectly by polynomial fitting to computed $\Xi_{k;\beta}(\mathbf{B})$ values as a function of $\mathbf{B}$. The fitting is simplified by the fact that only odd-orders of $\mathbf{B}$ enter in the expansion of $\Xi_{k;\beta}(\mathbf{B})$.

Before considering the benchmark calculations, we have in Fig. 4 plotted the VRG corrections to the oxygen shielding constant in H_2O against the integration cut-off parameter $\rho_{\text{cut-off}}$ (with hard and soft cut-offs) for the LHC, TP, and HHmod parameterizations of $g(\rho)$. Substantial variations in the corrections are observed and no convergence is achieved with reasonable cut-offs—in particular, for the LHC parameterization (with variations over about 60 ppm in the plot). The LDA- and BLYP-based VRG corrections are similar to each other for cut-offs larger than about 10^{-5}; for smaller cut-offs, the LDA-based corrections tend to be larger than the BLYP-based corrections. Moreover, the differences between the corrections obtained with hard and soft cut-offs are small compared with the differences observed for different cut-off parameters.

The TP correction is much better behaved, with variations on the order of 3.5 ppm and a consistent sign for the correction term. However, this variation and a lack of convergence with respect to varying the cut-off parameters mean that it cannot be recommended for practical use. The HHmod parameterization shows a large variation with regularization parameters and so also canot be recommended for practical use. However, it is interesting that for the large cut-off values HHmod leads to a negative correction, which is opposite in sign to the LHC and TP corrections with high cut-offs. This difference may reflect the qualitative difference in the functions $g(\rho)$ in Figures 1 and 2, in particular for large densities $g_{\text{HHmod}}(\rho)$ is positive, whilst $g_{\text{LHC}}(\rho)$ and $g_{\text{TP}}(\rho)$ are negative. This further re-enforces the need for an improved parameterization of $g(\rho)$—the stability of the functional obtained and the quality of the results is strongly influenced by this parameterization. Similar observations may be made for all molecules in our data set, whilst this set consists of only 27 molecules the results indicate that the lack of convergence with respect to regularization parameters seems to be a consistent issue, limiting the practical utility of VRG based functionals.

With these caveats in mind, we consider the nuclear shieldings calculated for the 27 molecules in our benchmark set at the same levels of theory and with the same parameterizations (with a hard cut-off $\rho_{\text{cut-off}} = 3.1 \times 10^{-4} \equiv r_s = 9.1055$) as for the magnetizabilities in Sec. IV A. In Fig. 5,

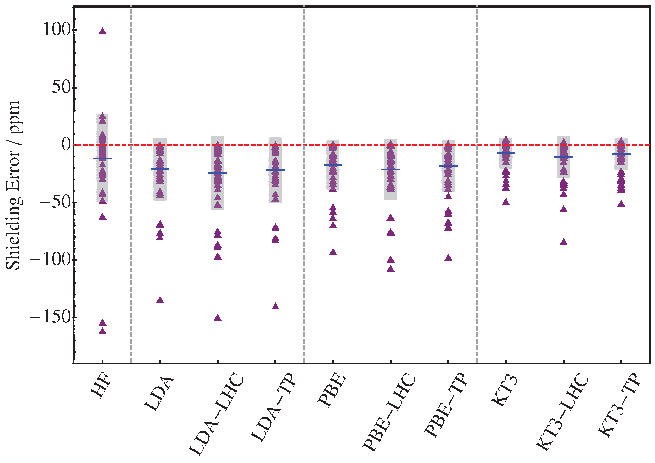

FIG. 5. Illustration of the errors in isotropic shielding constants (ppm) calculated using DFT functionals with and without the VRG(LHC) and VRG(TP) corrections in the aug-cc-pCVTZ basis set. Results that failed to converge during the SCF optimization with the VRG(LHC) correction have been omitted. The grey boxes enclose one sample standard deviation above and below the mean error. The mean error for each method is indicated by a horizontal blue line. The plot markers show the individual errors for each chemically unique nuclei in the 19 molecules listed in Sec. IV (a total of 48 data points).

we present the data for chemically unique nuclei in the subset of 19 molecules defined in Sec. IV (a total of 48 data points); all values are available in the supplementary material.[48] We note that the Kohn–Sham DFT shielding constants for LDA and PBE do not represent a substantial improvement over the Hartree–Fock constants, although they have a smaller spread their mean errors are in general worse. The KT3 functional does lead to a small improvement in both the mean error and a more significant improvement in the spread of the values. The overall trend is consistent with that observed in Ref. 12.

However, as for the magnetizabilities in Fig. 3, the addition of the VRG correction does not improve the calculated shieldings—in fact their quality tends to deteriorate with the application of VRG correction to the functional, especially for the LHC parameterization. These results are in line with the early observations of Lee, Handy, and Colwell[23] and indicate that (at least at the GGA level) improvement of the underlying functional to describe NMR properties, as is the case for KT3, does not lead to any significant difference when the associated VRG correction is calculated. The interplay between the choice of functional and the quality of VRG-type corrections beyond the GGA level remains to be investigated in future work.

V. (C)DFT BEYOND THE PERTURBATIVE REGIME

The availability of accurate current-density functionals would facilitate the study of molecules in very strong magnetic fields such as those encountered around white dwarf stars and magnetars.[49] Such strong fields may have a dramatic impact on the physics and chemistry of small molecules. Several studies have applied quantum-chemical methods such as the Hartree–Fock and FCI methods to small atoms as well as one- and two-electron molecular systems.[50–56] Such systems have also been studied with methods constructed for very high-accuracy.[57] Larger systems have been explored using density functionals based on asymptotic estimates for energies.[58,59]

On a technical note, very strong magnetic fields, $B \gg 1$ a.u. $= 2.35 \times 10^5$ T result in a substantial deformation and compression of atomic orbitals.[56,60–62] In such fields, traditional (isotropic) Gaussian-type orbitals are ill suited for the expansion of the electronic wave function. In the present work, we use conventional quantum-chemical Gaussian-type basis sets. As a result, we are limited to field strengths up to $B \sim 1$ a.u., for which the orbital deformation may be handled by decontracting the basis set and adding polarization functions.

An interesting phenomenon that can be addressed within the present computational limitations is the quality of (C)DFT approximations in describing chemical bonding and molecular orientation in magnetic fields. In magnetic fields $B \sim 1$ a.u., molecules that are otherwise unstable such as H_2 in the triplet state become stable, with a favoured orientation in the field.[4,6,56] In Ref. 6, this phenomenon was explained in terms of a new chemical bonding mechanism, perpendicular paramagnetic bonding, that arises from a stabilization of antibonding orbitals in a perpendicular orientation relative to the magnetic field. Hartree–Fock and FCI calculations have shown that this bonding is present in triplet H_2 and singlet He_2. Moreover, calculations at the Hartree–Fock level (which gives a qualitatively but not quantitatively correct description for paramagnetic bonding) on singlet helium clusters up to size He_6 indicate this bonding mechanism is not restricted to diatomic molecules.

Figures 6 and 7 show dissociation curves for the helium dimer subject to parallel and perpendicular fields of strength $B = 1$ a.u. The Hartree–Fock and FCI results are shown together with results obtained with standard (C)DFT functionals. The u-aug-cc-pVTZ basis set, where u stands for uncontracted, equipped with London orbital factors, was used. The dimer has a weak minimum for both parallel and perpendicular magnetic fields. The Hartree–Fock model underbinds, while all tested DFT functionals overbind. By symmetry, the

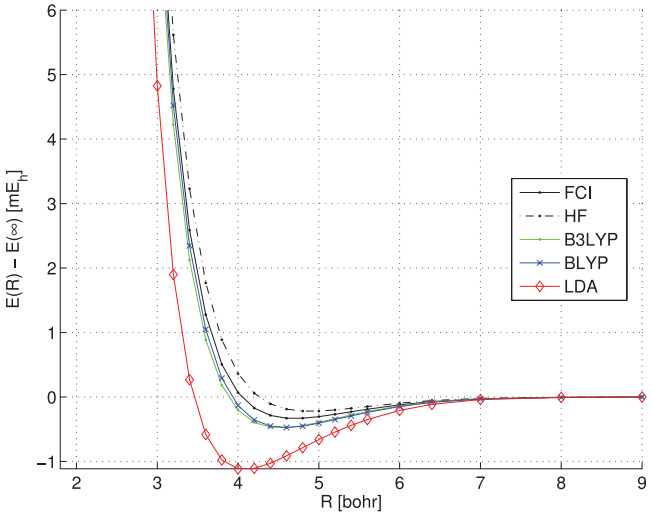

FIG. 6. Dissociation curves for He_2 subject to a parallel field $B_\parallel = 1$ a.u. The u-aug-cc-pVTZ basis set was used. Note that the curves have been aligned at $R = 9$ bohrs.

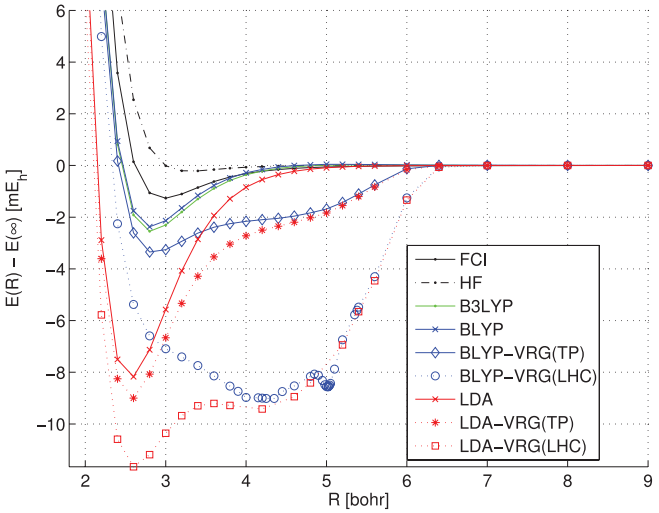

FIG. 7. Dissociation curves for He_2 subject to a perpendicular field $B_\perp = 1$ a.u. The u-aug-cc-pVTZ basis set was used. Note that the curves have been aligned at $R = 9$ bohrs.

vorticity vanishes for parallel fields. A vorticity-dependent VRG-type functional consequently vanishes too in this case.

For perpendicular fields, however, the vorticity does not vanish—see the dissociation curves for conventional and vorticity-dependent functionals in Fig. 7. (The vorticity-dependent functionals were regularized by a soft cut-off $\epsilon = 2.3873 \times 10^{-4}$ a.u., which corresponds to $r_s = 10$ a.u., in these calculations.) While the Hartree–Fock model and conventional DFT functionals show similar under- and overbinding, respectively, the addition of the VRG(LHC) and VRG(TP) functionals only degrade the accuracy. Both the depth and location of the minima become less accurate, with spurious plateaus appearing in the dissociation curves.

This behaviour may be understood from the observation that the vorticity vanishes for perpendicular fields in the dissociation and united-atom limits. Hence, the effect of the vorticity may be expected to be largest at intermediate bond lengths perpendicular to the field. Qualitatively, this behaviour is similar to the energetic preference introduced by the perpendicular paramagnetic bonding mechanism.[6] The VRG functionals tested thus show a spurious bias towards this bonding.

The SCF Kohn–Sham optimization appears to be more difficult when VRG functionals are used. Our implementation, which relies on a standard DIIS method, often finds states above the ground state when VRG functionals are used. We have dealt with this problem by starting the SCF optimization from different density matrices—for example, obtained by projection from a calculation with a different functional or different geometry.

Neither the tested conventional functionals (LDA, BLYP, B3LYP, and KT3) nor the VRG functionals (LHC and TP) were constructed for use with very strong magnetic fields. Whilst Hartree–Fock theory tends to lead to an under-binding, the standard LDA, BLYP and B3LYP tend to over-bind. For LDA this error is dramatic and similar to those observed in the absence of magnetic fields. The GGAs improve the situation but do not fully correct the error. By contrast, the VRG(LHC) and VRG(TP) corrected functionals are much less robust, leading to an exaggeration of this over-binding effect and the introduction of spurious features on the potential energy curve. At least the VRG(TV) functional is likely to share this problem, since its model function $g_{TV}(\rho)$ is similar to $g_{LHC}(\rho)$ and $g_{TP}(\rho)$.

Higuchi and Higuchi's functional,[27,28] modified as described above, is based on a model $g_{HH}(\rho)$ that is rather different from the other functionals studied. The contribution from VRG(HHmod) produces a purely dissociative potential energy curve for perpendicular fields (data not shown). Since the VRG(HHmod) functional gives errors in the opposite direction compared to the VRG(LHC) and VRG(TP) functionals, an interesting possibility is to try to fit a parameterization flexible enough to interpolate between these functionals to benchmark data.

VI. CONCLUSIONS

We have reported an implementation of DFT and CDFT for molecular calculations in magnetic fields. The implementation has several novel features: First, external magnetic fields are treated non-perturbatively, enabling both static response quantities and intrinsically non-perturbative phenomena to be investigated. Second, London atomic orbitals are used in conjunction with finite magnetic fields to achieve gauge-origin invariance and faster basis-set convergence. Third, the treatment of the current-dependent contribution to the exchange-correlation functional is fully self-consistent.

Our DFT implementation has been demonstrated by computing magentizabilities, NMR shielding constants and hypermagnetizabilities for a set of small molecules. The CDFT implementation has been used to explore the accuracy of several parametrizations of the vorticity-dependent VRG functionals. For magnetizabilities and nuclear shielding constants, these functionals tend to degrade accuracy compared to conventional DFT functionals. Also the description of the non-perturbative phenomenon of perpendicular paramagnetic bonding degrades when the VRG functional is added. Although these functionals were constructed to account for the effects of external magnetic fields, a common problem is that the parameter values have been selected to describe a uniform electron gas in the medium to high-density regime (i.e., $r_s \leq 10$ or $r_s \leq 20$). The low-density limit, which is important in molecular calculations, is thus left underdetermined. The asymptotic decay of $\sim\rho^{-1/3}\nu^2$ seen in the presently available parametrizations appears to be too slow for molecular calculations, making regularization necessary. Moreover, results obtained with the VRG functionals are too sensitive to the choice of regularization parameter to be useful.

Interestingly, a modified version Higuchi and Higuchi's functional,[27,28] reparametrized so as to have a useful low-density behaviour, stands out from the other VRG functionals. It decays as $\sim\rho\nu^2$, which is substantially faster, and because it has the opposite sign in the medium to high-density regime compared to the VRG(LHC) and VRG(TP) functionals, for example, it yields errors in the opposite direction. The latter point raises the tempting possibility of attempting to fit an interpolation between VRG(HHmod) and VRG(LHC) or VRG(TP) to benchmark data.

There are several possible directions for future work on improved CDFT corrections. First, as already discussed, the form of the $g(\rho)$ parameterization warrants further investigation, particularly in light of the strong sensitivity of the results and functional stability to these parameterizations. The generation of accurate data at the FCI or coupled-cluster levels at different field strengths using the LONDON program may provide a useful way to tailor these parameterizations for practical use. Second, the development of corrections appropriate for addition to functionals beyond the GGA level can be pursued and should lead to a better understanding of the interplay between errors in the CDFT corrections and the underlying functionals. Finally, to circumvent difficulties with the vorticity it may be fruitful to consider other quantities on which CDFT corrections may be constructed, such as the form of Eq. (8). In all of these areas the present CDFT implementation should provide a useful test bed for new CDFT approximations.

ACKNOWLEDGMENTS

This work was supported by the Norwegian Research Council through the CoE Centre for Theoretical and Computational Chemistry (CTCC) Grant Nos. 179568/V30 and 171185/V30 and through the European Research Council under the European Union Seventh Framework Program through the Advanced Grant ABACUS, ERC Grant Agreement No. 267683. A.M.T. is also grateful for support from the Royal Society University Research Fellowship scheme.

APPENDIX: PARAMETRIZATIONS OF $g(\rho)$

In this appendix, we collect all parametrizations of $g(\rho)$ plotted in Fig. 1. For consistency of presentation, the notation has been modified from the original papers. Atomic units are used.

Introducing the Fermi momentum $k_F = (3\pi^2\rho)^{1/3}$ and the Wigner–Seitz radius $r_s = (4\pi\rho/3)^{-1/3}$, the original VRG parametrization of Refs. 8 and 21 is given by

$$g_{\text{orig}}(\rho) = \frac{1}{24\pi^2}k_F(0.02764 r_s \ln r_s + 0.01407 r_s), \tag{A1}$$

where the first constant comes from an analytical expression: $(9\pi/4)^{-1/3}/(6\pi) \approx 0.02764$.

The LHC parameterization of the VRG functional is given by

$$g_{\text{LHC}}(\rho) = -\frac{1}{24\pi^2}k_F[1 - e^{-a_0 r_s}(a_1 + a_2 r_s)], \tag{A2}$$

with $a_0 = 0.042$, $a_1 = 1$, and $a_2 = 0.028$.[23] Orestes, Marcasso, and Capelle[24] presented a three-term fit and a five-term fit of the VRG integrand, the latter OMC fit being given by

$$g_{\text{OMC}}(\rho) = -\frac{1}{24\pi^2}k_F[1 - C^{\text{OMC}}(\rho)], \tag{A3}$$

with

$$C^{\text{OMC}}(\rho) = 1.038 - 0.4990 r_s^{1/3} + 0.4423\sqrt{r_s} - 0.06696 r_s + 0.0008432 r_s^2. \tag{A4}$$

The TP parameterization is defined by[25]

$$g_{\text{TP}}(\rho) = -\frac{1}{24\pi^2}k_F[1 - \bar{C}^{\text{TP}}(\rho)], \tag{A5}$$

with

$$C_1^{\text{TP}}(\rho) = 1 + 0.027643 r_s \log r_s, \tag{A6}$$

$$C_2^{\text{TP}}(\rho) = C^{\text{OMC}}(\rho) = 1.1038 - 0.4990 r_s^{1/3} + 0.4423\sqrt{r_s} - 0.06696 r_s + 0.0008432 r_s^2, \tag{A7}$$

$$C_3^{\text{TP}}(\rho) = (1 + 0.027 r_s) e^{-0.041 r_s}, \tag{A8}$$

$$\bar{C}^{\text{TP}}(\rho) = \left[C_1^{\text{TP}} e^{-2.8 r_s} + (1 - e^{-2.8 r_s}) C_2^{\text{TP}}\right] e^{-0.05 r_s} + (1 - e^{-0.05 r_s}) C_3^{\text{TP}}. \tag{A9}$$

Finally, the TV parameterization of the VRG functional is defined by[26]

$$g_{\text{TV}}(\rho) = -\frac{1}{24\pi^2}k_F[1 - \bar{C}^{\text{TV}}(\rho)], \tag{A10}$$

with

$$C_1^{\text{TV}}(\rho) = 1 + b_1 r_s \log r_s, \tag{A11}$$

$$C_2^{\text{TV}}(\rho) = b_3 + b_4 r_s^{1/3} + b_5\sqrt{r_s} + b_6 r_s + b_7 r_s^2, \tag{A12}$$

$$C_3^{\text{TV}}(\rho) = (1 + b_9 r_s) e^{-b_{10} r_s}, \tag{A13}$$

$$\bar{C}^{\text{TV}}(\rho) = \left[C_1^{\text{TV}} e^{-b_2 r_s} + C_2^{\text{TV}}(1 - e^{-b_2 r_s})\right] e^{-b_8 r_s} + (1 - e^{-b_8 r_s}) C_3^{\text{TV}}, \tag{A14}$$

where $b_1 = (9\pi/4)^{-1/3}/(6\pi)$, $b_2 = 2.5$, $b_3 = 1.1$, $b_4 = -0.49$, $b_5 = 0.438$, $b_6 = -0.07$, $b_7 = 0.00182$, $b_8 = 0.054$, $b_9 = 0.02$, and $b_{10} = 0.05$.

The Higuchi–Higuchi parameterization is given by[27,28]

$$g_{\text{HHx}}(\rho) = 2D_x, \tag{A15}$$

$$g_{\text{HHc}}(\rho) = 2C_0 e^{-\alpha\rho}\frac{\rho^3}{(\rho - \delta)^3}, \tag{A16}$$

$$g_{\text{HH}}(\rho) = g_{\text{HHx}}(\rho) + g_{\text{HHc}}(\rho), \tag{A17}$$

where $\alpha = 0.653$, $D_x = 3.76 \times 10^{-4}$, $C_0 = -4.669 \times 10^{-4}$, and $\delta = 10^{-30}$. In our modified functional, HHmod, the value of D_x was changed to $D_x = -C_0 = 4.669 \times 10^{-4}$ to ensure a useful low-density limit. We have also set $\delta = 0$, since this makes no difference, to within normal numerical precision, in regions where $\rho \gg 10^{-30}$ and inclusion of regions where $\rho \approx 10^{-30}$ would make the original exchange-correlation energy ill-defined.

[1] T. Helgaker, M. Jaszuński, and K. Ruud, Chem. Rev. **99**, 293 (1999).
[2] T. Helgaker, S. Coriani, P. Jørgensen, K. Kristensen, J. Olsen, and K. Ruud, Chem. Rev. **112**, 543 (2012).

[3]E. I. Tellgren, A. Soncini, and T. Helgaker, J. Chem. Phys. **129**, 154114 (2008).
[4]E. I. Tellgren, S. S. Reine, and T. Helgaker, Phys. Chem. Chem. Phys. **14**, 9492 (2012).
[5]E. I. Tellgren, T. Helgaker, and A. Soncini, Phys. Chem. Chem. Phys. **11**, 5489 (2009).
[6]K. K. Lange, E. I. Tellgren, M. R. Hoffmann, and T. Helgaker, Science **337**, 327 (2012).
[7]C. J. Grayce and R. A. Harris, Phys. Rev. A **50**, 3089 (1994).
[8]G. Vignale and M. Rasolt, Phys. Rev. Lett. **59**, 2360 (1987).
[9]G. Vignale and M. Rasolt, Phys. Rev. B **37**, 10685 (1988).
[10]K. Capelle and G. Vignale, Phys. Rev. B **65**, 113106 (2002).
[11]O. B. Lutnæs, A. M. Teale, T. Helgaker, D. J. Tozer, K. Ruud, and J. Gauss, J. Chem. Phys. **131**, 144104 (2009).
[12]A. M. Teale, O. B. Lutnæs, T. Helgaker, D. J. Tozer, and J. Gauss, J. Chem. Phys. **138**, 024111 (2013).
[13]K. Capelle and E. K. U. Gross, Phys. Rev. Lett. **78**, 1872 (1997).
[14]M. Taut, P. Machon, and H. Eschrig, Phys. Rev. A **80**, 022517 (2009).
[15]E. H. Lieb and R. Schrader, Phys. Rev. A **88**, 032516 (2013); e-print arXiv:1308.2664v1.
[16]E. Cancès, J. Chem. Phys. **114**, 10616 (2001).
[17]E. Cances, K. N. Kudin, G. E. Scuseria, and G. Turinici, J. Chem. Phys. **118**, 5364 (2003).
[18]E. Kraisler, G. Makov, N. Argaman, and I. Kelson, Phys. Rev. A **80**, 032115 (2009).
[19]C. R. Nygaard and J. Olsen, J. Chem. Phys. **138**, 094109 (2013).
[20]E. Tellgren, S. Kvaal, and T. Helgaker, "Fermion *N*-representability for prescribed density and paramagnetic current density;" e-print arXiv:1310.1246v2.
[21]G. Vignale, M. Rasolt, and D. J. W. Geldart, Phys. Rev. B **37**, 2502 (1988).
[22]A. M. Lee, S. M. Colwell, and N. C. Handy, Chem. Phys. Lett. **229**, 225 (1994).
[23]A. M. Lee, N. C. Handy, and S. M. Colwell, J. Chem. Phys. **103**, 10095 (1995).
[24]E. Orestes, T. Marcasso, and K. Capelle, Phys. Rev. A **68**, 022105 (2003).
[25]J. Tao and J. P. Perdew, Phys. Rev. Lett. **95**, 196403 (2005).
[26]J. Tao and G. Vignale, Phys. Rev. B **74**, 193108 (2006).
[27]K. Higuchi and M. Higuchi, Phys. Rev. B **74**, 195122 (2006).
[28]M. Higuchi and K. Higuchi, Phys. Rev. B **75**, 195114 (2007).
[29]W. Zhu and S. B. Trickey, Phys. Rev. A **72**, 022501 (2005).
[30]A. D. Becke, Can. J. Chem. **74**, 995 (1996).
[31]S. Pittalis, S. Kurth, S. Sharma, and E. K. U. Gross, J. Chem. Phys. **127**, 124103 (2007).
[32]J. F. Dobson, J. Chem. Phys. **98**, 8870 (1993).
[33]A. D. Becke, J. Chem. Phys. **88**, 2547 (1988).
[34]C. W. Murray, N. C. Handy, and G. J. Laming, Mol. Phys. **78**, 997 (1993).
[35]R. Lindh, P.-Å. Malmqvist, and L. Gagliardi, Theor. Chem. Acc. **106**, 178 (2001).
[36]V. Lebedev, Comput. Math. Math. Phys. **15**, 44 (1975).
[37]V. Lebedev, Comput. Math. Math. Phys. **16**, 10 (1976).
[38]V. Lebedev, Sib. Math. J. **18**, 99 (1977).
[39]V. Lebedev and A. Skorokhodov, Russ. Acad. Sci. Dokl. Math. **45**, 587 (1992).
[40]V. Lebedev, Russ. Acad. Sci. Dokl. Math. **50**, 283 (1995).
[41]V. Lebedev and D. Laikov, Dokl. Math. **59**, 477 (1999).
[42]K. Aidas, C. Angeli, K. L. Bak, V. Bakken, R. Bast, L. Boman, O. Christiansen, R. Cimiraglia, S. Coriani, P. Dahle, E. K. Dalskov, U. Ekström, T. Enevoldsen, J. J. Eriksen, P. Ettenhuber, B. Fernández, L. Ferrighi, H. Fliegl, L. Frediani, K. Hald, A. Halkier, C. Hättig, H. Heiberg, T. Helgaker, A. C. Hennum, H. Hettema, E. Hjerteniæs, S. Høst, I.-M. Høyvik, M. F. Iozzi, B. Jansík, H. J. Å. Jensen, D. Jonsson, P. Jørgensen, J. Kauczor, S. Kirpekar, T. Kjærgaard, W. Klopper, S. Knecht, R. Kobayashi, H. Koch, J. Kongsted, A. Krapp, K. Kristensen, A. Ligabue, O. B. Lutnæs, J. I. Melo, K. V. Mikkelsen, R. H. Myhre, C. Neiss, C. B. Nielsen, P. Norman, J. Olsen, J. M. H. Olsen, A. Osted, M. J. Packer, F. Pawlowski, T. B. Pedersen, P. F. Provasi, S. Reine, Z. Rinkevicius, T. A. Ruden, K. Ruud, V. Rybkin, P. Sałek, C. C. M. Samson, A. Sánchez de Merás, T. Saue, S. P. A. Sauer, B. Schimmelpfennig, K. Sneskov, A. H. Steindal, K. O. Sylvester-Hvid, P. R. Taylor, A. M. Teale, E. I. Tellgren, D. P. Tew, A. J. Thorvaldsen, L. Thøgersen, O. Vahtras, M. A. Watson, D. J. D. Wilson, M. Ziolkowski, and H. Ågren, "The Dalton quantum chemistry program system," WIREs Comput. Mol. Sci. (published online).
[43]*DALTON*, a molecular electronic structure program, Release Dalton 2013.0, 2013, see http://daltonprogram.org.
[44]U. Ekström, L. Visscher, R. Bast, A. J. Thorvaldsen, and K. Ruud, J. Chem. Theory Comput. **6**, 1971 (2010).
[45]W. Zhu and S. B. Trickey, J. Chem. Phys. **125**, 094317 (2006).
[46]G. I. Pagola, M. C. Caputo, M. B. Ferraro, and P. Lazzeretti, Phys. Rev. A **74**, 022509 (2006).
[47]G. I. Pagola, S. Pelloni, M. C. Caputo, M. B. Ferraro, and P. Lazzeretti, Phys. Rev. A **72**, 033401 (2005).
[48]See supplementary material at http://dx.doi.org/10.1063/1.4861427 for the magnetizability, hyper-magnetizability, and NMR shielding constants calculated in this work.
[49]D. Lai, Rev. Mod. Phys. **73**, 629 (2001).
[50]T. Detmer, P. Schmelcher, and L. S. Cederbaum, Phys. Rev. A **57**, 1767 (1998).
[51]P. Schmelcher, M. V. Ivanov, and W. Becken, Phys. Rev. A **59**, 3424 (1999).
[52]P. Schmelcher, T. Detmer, and L. S. Cederbaum, Phys. Rev. A **61**, 043411 (2000).
[53]W. Becken and P. Schmelcher, Phys. Rev. A **65**, 033416 (2002).
[54]O.-A. Al-Hujaj and P. Schmelcher, Phys. Rev. A **70**, 023411 (2004).
[55]A. Luhr, O.-A. Al-Hujaj, and P. Schmelcher, Phys. Rev. A **75**, 013403 (2007).
[56]A. Kubo, J. Phys. Chem. A **111**, 5572 (2007).
[57]A. Ishikawa, H. Nakashima, and H. Nakatsuji, Chem. Phys. **401**, 62 (2012).
[58]Z. Medin and D. Lai, Phys. Rev. A **74**, 062507 (2006).
[59]Z. Medin and D. Lai, Phys. Rev. A **74**, 062508 (2006).
[60]U. Kappes and P. Schmelcher, J. Chem. Phys. **100**, 2878 (1994).
[61]P. Schmelcher and L. S. Cederbaum, Phys. Rev. A **37**, 672 (1988).
[62]Y. P. Kravchenko and M. A. Lieberman, Int. J. Quantum Chem. **64**, 513 (1997).
[63]J. P. Perdew, K. Burke, and M. Ernzerhof, Phys. Rev. Lett. **77**, 3865 (1996).
[64]T. W. Keal and D. J. Tozer, J. Chem. Phys. **121**, 5654 (2004).